

ENGR 406 MicroElectroMechanical Engineering

Documentation Package



Students:

Robson Wong (67139360)

Will Tanner (26081869)

Matthew Day (47204565)

Daniel Holmes (68152776)

School of Engineering

Faculty of Applied Science

The University of British Columbia Okanagan

2023-12-11

Table of Contents

List of Figures:	3
Nomenclature:	4
1.0 Introduction.....	5
2.0 Literature Search.....	6
3.0 Design Description.....	8
4.0 Test Plan.....	15
5.0 Results.....	16
6.0 Conclusion and Lessons Learned.....	20
7.0 References:	21
8.0 Appendix:	21

List of Figures:

Figure 1.1 - Unactivated Structure.....	5
Figure 1.2 - Activated Structure (Base focal view).....	5
Figure 1.3 - Activated Structure (platform focal view).....	5
Figure 2.1 - Advanced sensor used by Sturm et al.....	7
Figure 2.2- Recirculating zone inside separation bubble.....	7
Figure 3.01 - Assembled Macromodel 1	
Figure 3.02 - Macromodel 2.....	8
Figure 3.1 - Latching Cantilever.....	8
Figure 3.2 - Elevated Center Platform.....	9
Figure 3.3 - Ratcheting Cantilever.....	9
Figure 3.4 - Device Subcomponents.....	9
Figure 3.5 - Assembly Force Vectors.....	10
Figure 3.6 - SU8_1 with 20 micron thickness (Round 1).....	10
Figure 3.7 - SU8_1 with 30 micron thickness (Round 2).....	11
Figure 3.8 - SU8_2 with 30 micron thickness (Round 2).....	11
Figure 3.9 - SU8_2 with 50 micron thickness (Round 2).....	12
Figure 3.10 - Short Cantilever (600 micron).....	12
Figure 3.11 - Long Cantilever (1000 micron).....	12
Figure 3.12 -Platform Vertical Wandering.....	13
Figure 3.13 - Angled Connecting Beams.....	13
Figure 3.15 - Design Layout 2.....	14
Figure 5.1: Activated Structure (platform focal view).....	16
Figure 5.2 - Activated Structure (Base focal view).....	16
Figure 5.3 - Partially constructed structure (Base focal view).....	17
Figure 5.4 - Stress concentration at notch.....	17
Figure 5.5 - Hot-Wire Anemometry.....	18
Figure 5.6 - Measurement of Resistance for Activated Gold Plated Structure.....	18
Figure 5.7 - Power Dissipation Model.....	19
Figure 5.8 - Power Dissipation Model Without Cooling.....	19

Nomenclature:

$\omega(x)$ = Transverse deflection of the cantilever
k = Stiffness of the cantilever
x = Position along the cantilever
L = Length of Cantilever
 x_h = Position of maximum height displacement along the cantilever
 x_σ = Position of maximum stress along the cantilever
 $\sigma_{max}(x)$ = Maximum Stress
 $M(x)$ = Bending moment
c = Maximum Fibre distance
I = second moment of inertia of the cantilever
E = Modulus of Elasticity
 α = Thermal expansion coefficient
T = Temperature of thermal element
 T_0 = Ambient temperature of thermal element
R = Resistance of a thermal element @ T
 R_0 = Resistance of a thermal element @ T_0

1.0 Introduction

MEMS, or Micro-Electro-Mechanical Systems, play a crucial role in contemporary technology, significantly influencing various industries and applications. Whether it's the accelerometers in automotive airbags or the diverse array of sensors within your mobile device, MEMS contribute to creating a safer and improved world for humanity.

Our project delved into the intricacies of designing and manufacturing MEMS structures. We were tasked with creating a simple MEMS structure using 4 lithographic layers, a Chromium/Aluminum sacrificial layer, two SU8 structural layers, and one conductive layer of Chromium/Gold. We were given two opportunities to fabricate and test our device, so only one chance to improve upon our design based on the results of our first test.

The primary objective of this project was to develop a deployable MEMS structure designed to theoretically gauge fluid velocity across a surface. Our design featured two interlocking cantilevers positioned in opposition of each other. When activated, these cantilevers would elevate a platform above the surface, effectively mitigating the zero-slip condition that occurs at the body's surface. An activated structure can be observed in Figures 1.1 to 1.3. The device measures the change in airflow by using the change in resistance due to convection heat loss. It can also function as a bistable platform to raise an object off the substrate for further testing. Our goals were to optimize the stability of the platform, the height of the platform above the substrate, the reliability of assembly, and the range of airflow measured.

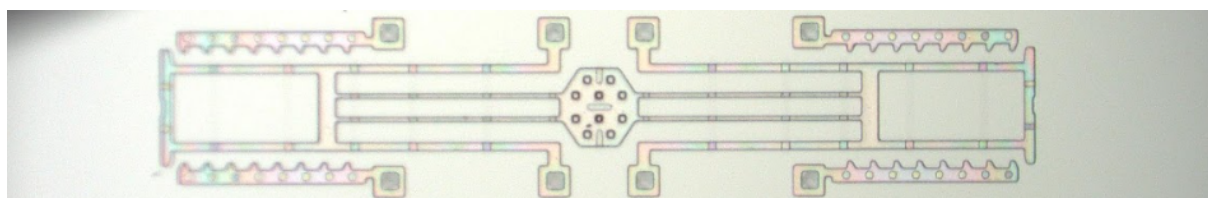


Figure 1.1 - Unactivated Structure

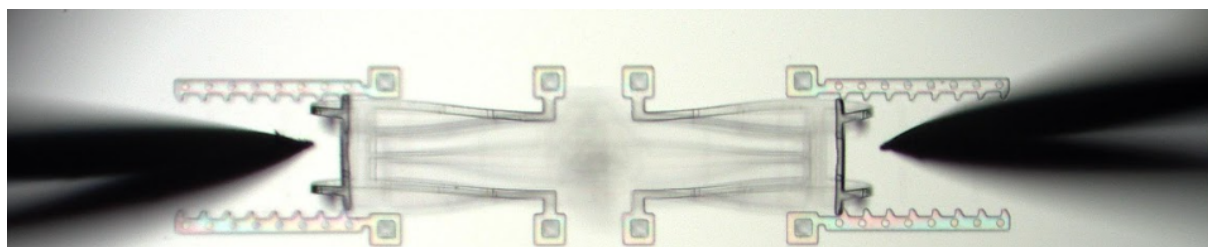


Figure 1.2 - Activated Structure (Base focal view)

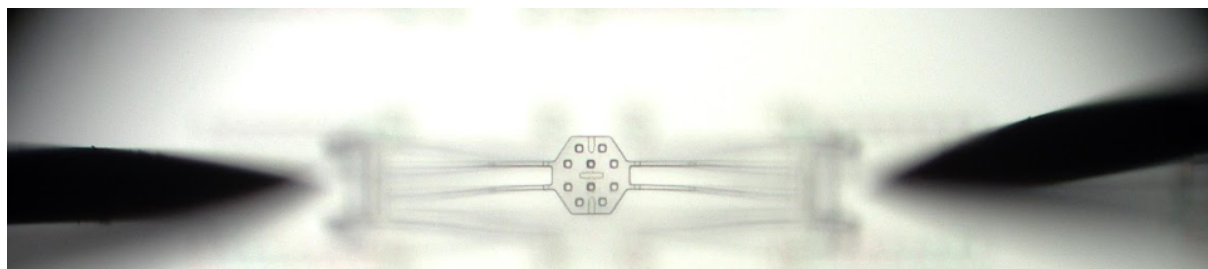


Figure 1.3 - Activated Structure (platform focal view)

2.0 Literature Search

For our project we looked at the buckled cantilevers for out-of-plane platforms written by R W Johnstone, A H Ma, D Sameoto, M Parameswaran and A M Leung. This paper covers several important factors highlighting the mechanical characteristics of a buckled cantilever. The most important points the paper covered with respect to our project described the location of the maximum height displacement and maximum stress along the buckled cantilever.

In order to find the maximum height displacement of the buckled cantilever, the extrema of the mode-shape needs to be found. Using the linear beam-bending theory the mode-shape of the buckled cantilever can be found.

$$\omega(x) = \sin(kx) - kL\cos(kx) + kL(1 - x/L)$$

Taking the extrema of the mode-shape, knowing that the base of the cantilever is fixed, reducing the problem to:

$$\omega'(x) = 0$$

Which results in the following solutions:

$$x_h = 0$$

$$x_h = 0.6017L$$

This concludes that attaching a platform 60.17% along the length of the cantilever will provide the maximum height displacement.

In order to find the location of maximum stress along the buckled cantilever, the equation for the maximum stress in the cantilever needs to be examined.

$$\sigma_{max}(x) = \frac{Mc}{I} = \frac{c}{I}|M(x)| = \frac{c}{I}\left| - EI \frac{d^2\omega(x)}{dx^2} \right| = Ec\left| \frac{d^2\omega(x)}{dx^2} \right|$$

Taking the extrema of the second derivative results in

$$x_\sigma = 0.6504L$$

This concludes that the point of maximum stress occurs 65.04% along the length of the cantilever.

We also examined “Boundary Layer Separation and Reattachment Detection on Airfoils by Thermal Flow Sensors” by Hannes Sturm 1,Gerrit Dumstorff 1,Peter Busche 2,Dieter Westermann 2 and Walter Lang 1. This paper explained how they were implementing similar sensors for boundary layer analysis. We used this for reference for applications of our structure, and to tweak our designs to best match similar requirements to what they had.

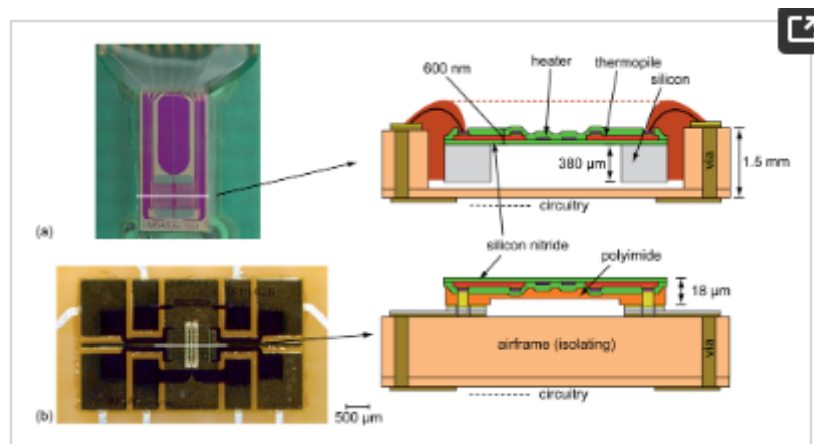


Figure 2.1 - Advanced sensor used by Sturm et al.

Sturm et al focused on measuring eddy currents occurring when the surface was moved and boundary conditions changed:

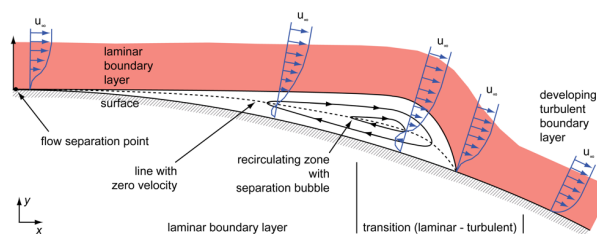


Figure 2.2- Recirculating zone inside separation bubble

This is important information because these bubbles result in a large decrease in aerodynamic efficiency, and should be minimized. Our design can be applied to a similar effect to find these bubbles.

3.0 Design Description

Our design underwent several iterations, featuring three core components: the elevated center platform, the latching cantilever, and the ratcheting cantilever mechanism, all depicted in the figures 3.1-3.3. Notably, each of these primary components contain various subcomponents (shown in figure 3.4), with modifications and refinements introduced in each iteration of our design process. Our initial approach was to create macro models to better discuss and evaluate ideas before generating our layouts and performing calculations. An example of this is seen in figures 3.01 to 3.02 where we discussed elongating the ratcheting jaws and slightly adjusting the cross beam to allow for the arm angle to change.

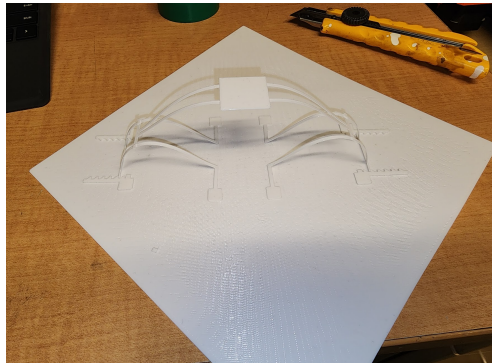


Figure 3.01 - Assembled Macromodel 1

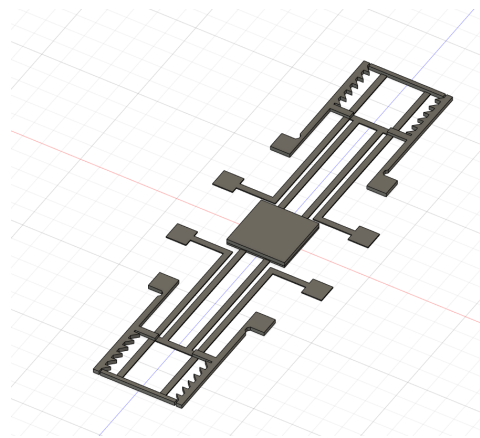


Figure 3.02 - Macromodel 2

After this stage we created out klayout iterations:

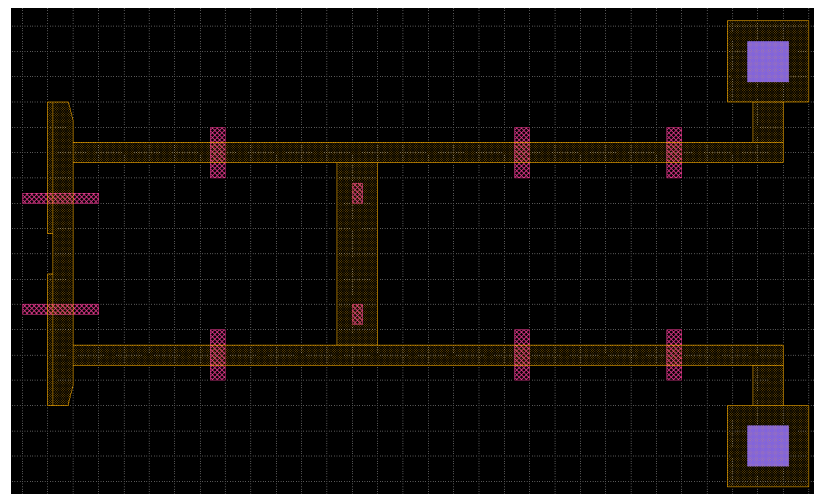


Figure 3.1 - Latching Cantilever

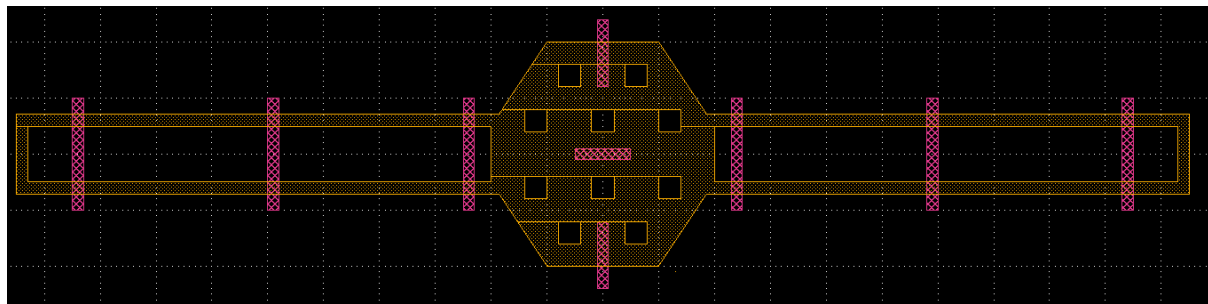


Figure 3.2 - Elevated Center Platform

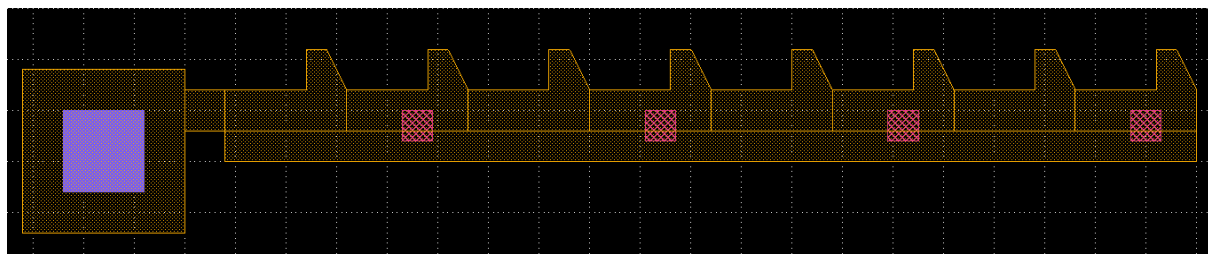


Figure 3.3 - Ratcheting Cantilever

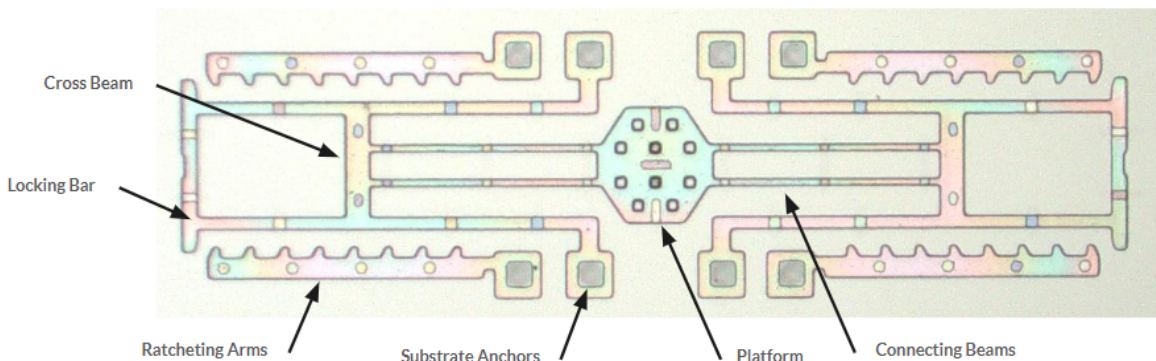


Figure 3.4 - Device Subcomponents

Our device could be assembled by pushing the locking bars towards the middle of the device, thus elevating the center platform as the latching cantilever displaced inwards. The secure engagement of the locking beams relies on the exact tolerance between the teeth on the ratcheting arms and the tips of the locking bar, along with the stiffness of the locking bar and ratcheting cantilevers. Recognizing this relationship enabled us to focus on refining these components through iterations.

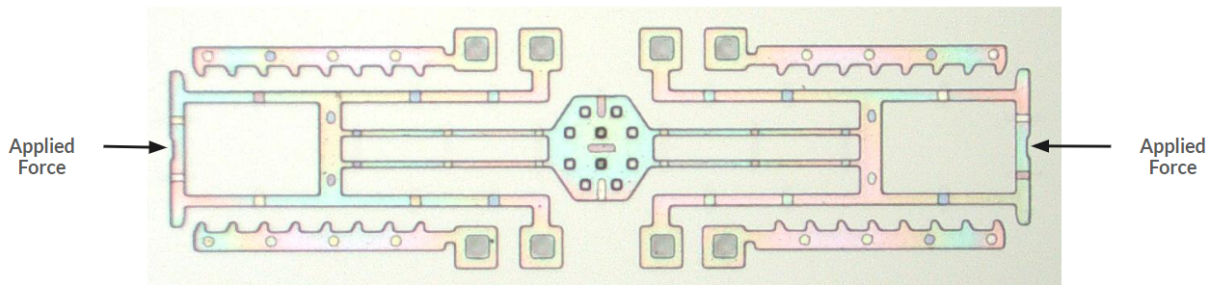


Figure 3.5 - Assembly Force Vectors

The success of assembly hinges on determining the spring constant of the ratcheting arms, a factor influenced by the thickness of the attachment points to the anchor. Throughout our design process, we experimented with varying this thickness to enhance mechanical stability (shown in figure 3.6-3.9). However, in our second design iterations (figure 3.7-9), we inadvertently surpassed the desired outcome by excessively increasing the thickness. This occurred because the moment of inertia of a rectangle increases by t^3 resulting in a substantial relative change increase — our 10-micron increment led to a 237.5% rise in stiffness, while the 30-micron increment resulted in a staggering 1462.5% (Equation 8.1). It's important to note that these calculations were made in hindsight, an error on our part.

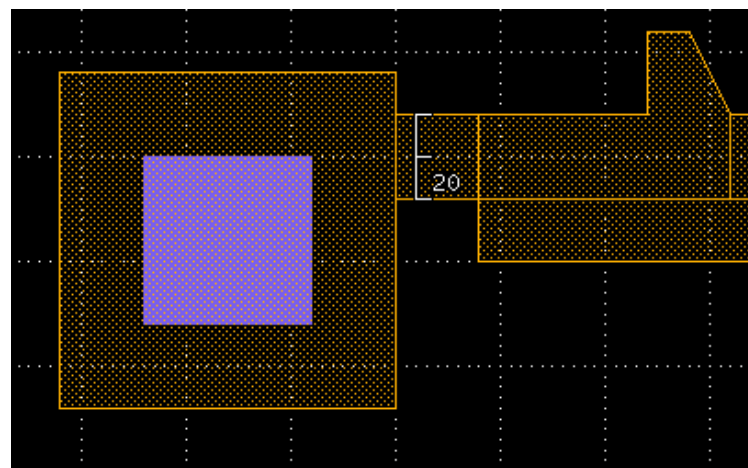


Figure 3.6 - SU8_1 with 20 micron thickness (Round 1)

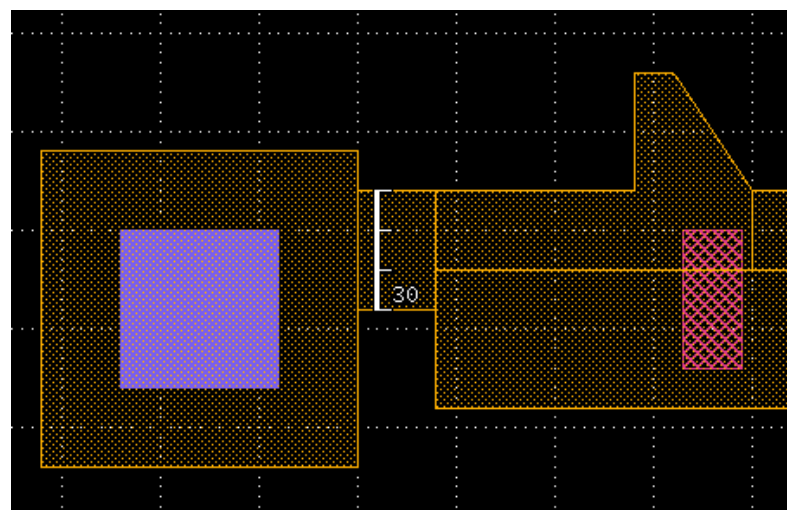


Figure 3.7 - SU8_1 with 30 micron thickness (Round 2)

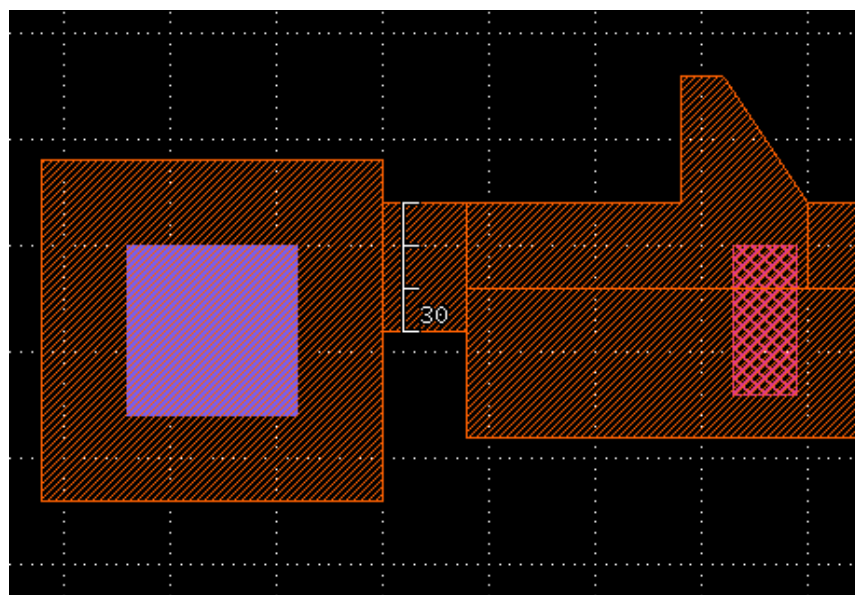


Figure 3.8 - SU8_2 with 30 micron thickness (Round 2)

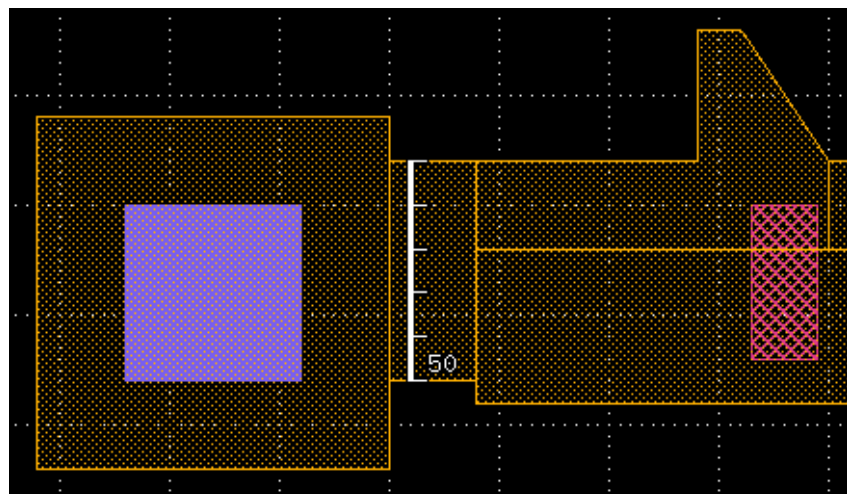


Figure 3.9 - SU8_2 with 50 micron thickness (Round 2)

To obtain a maximum height for our platform, we found from our literary search that the placement of our cross beam should be at 60.17% of the length of our cantilever. This placement can be shown in our long and short designs below. Our short cantilever design was 700 micron long, resulting in the placement of our cross bar at 420 micron, and our long cantilever design 1000 micron long, resulting in the placement at 600 micron.

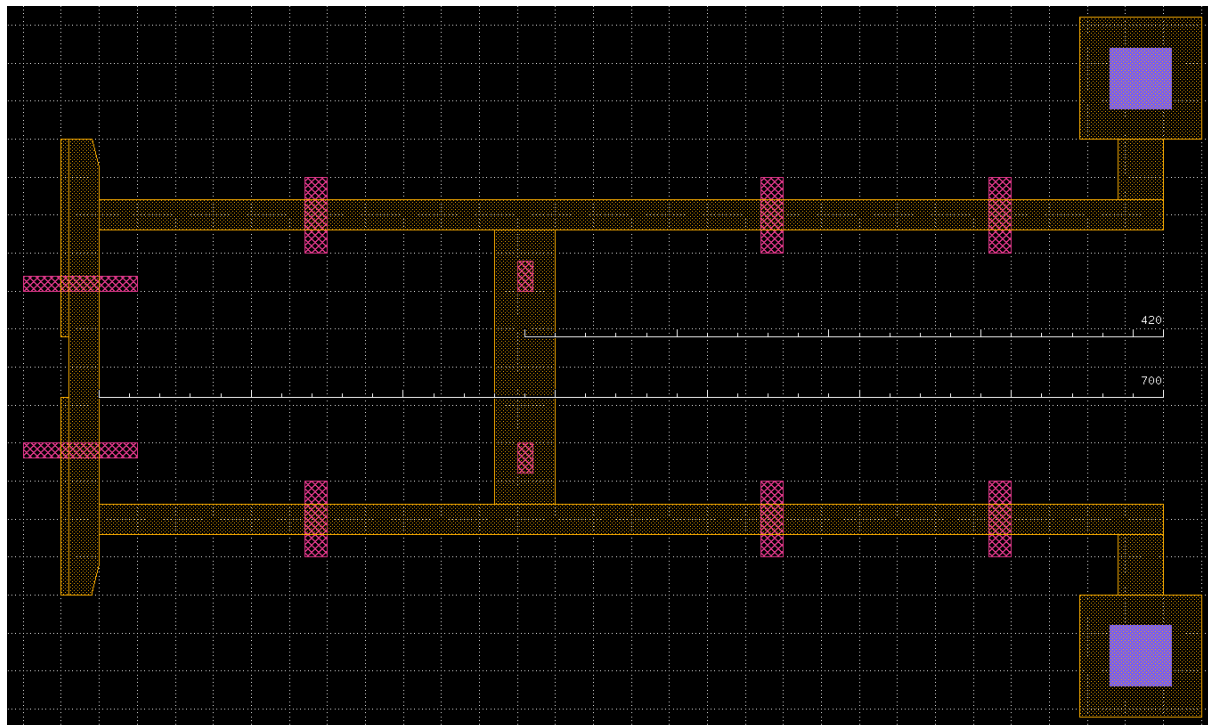


Figure 3.10 - Short Cantilever (600 micron)

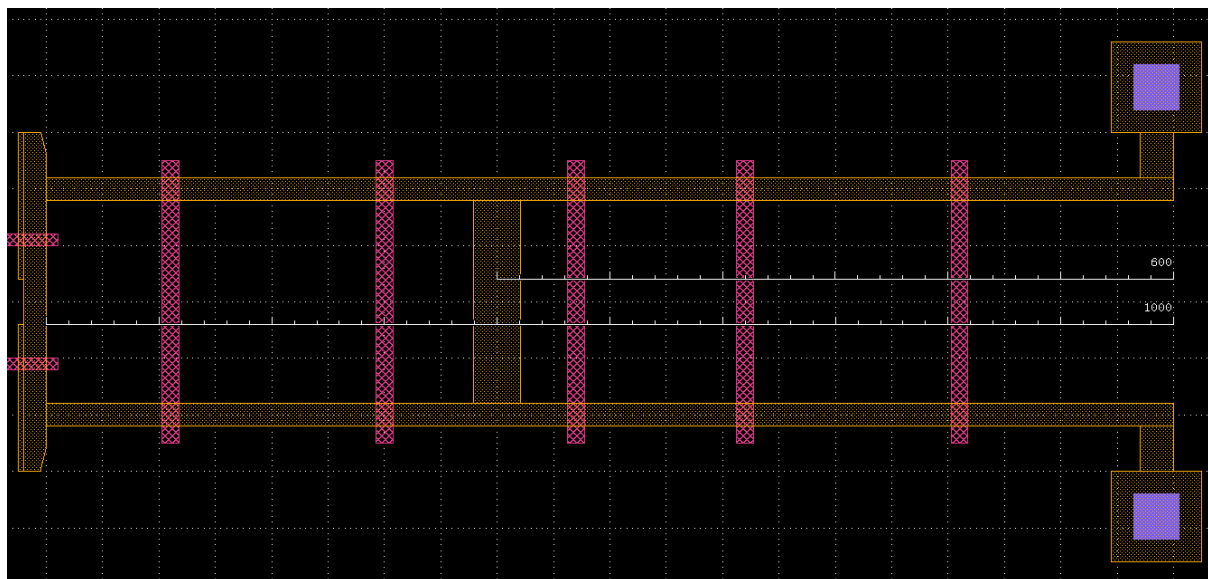


Figure 3.11 - Long Cantilever (1000 micron)

Another design iteration that we implemented in our second layout was angling the connecting beams from the cross beam to the platform. This change was instigated by the observation of the platform's vertical deflection. By adding slight angles to the connecting

beams, we'd hope that the platform's stability would increase, thus providing a better stage for flow measurements.

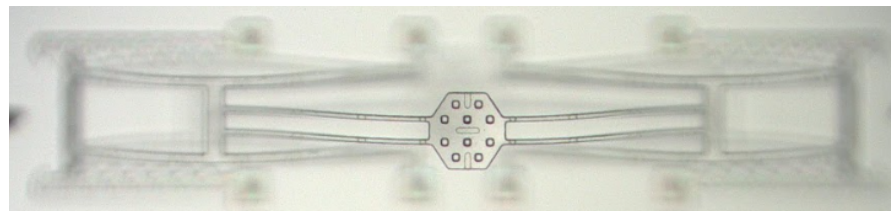


Figure 3.12 -Platform Vertical Wandering

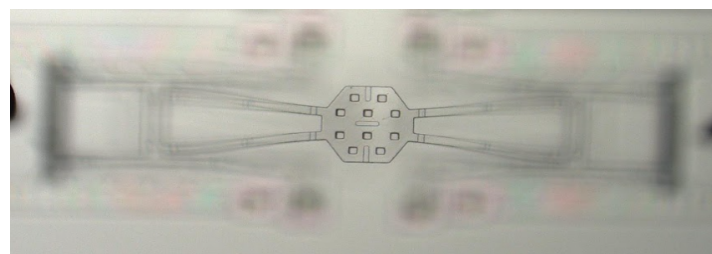


Figure 3.13 - Angled Connecting Beams

An overview of our design iterations can be observed in our first and second mask profiles shown in the figures below. Due to the limited space of our layout (5000 micron by 5000 micron area), we only created one pair of every iteration. This format maximized the amount of iterations we could test while also creating a backup in the case of device failure.

Things to note; in the layouts are the use of SU8_2 for the platform iterations in the first design layout and for the ratcheting arms in the second design layout. The different lengths of structures can be observed in both iterations as well as a scaled version of the smaller device in the second layout.

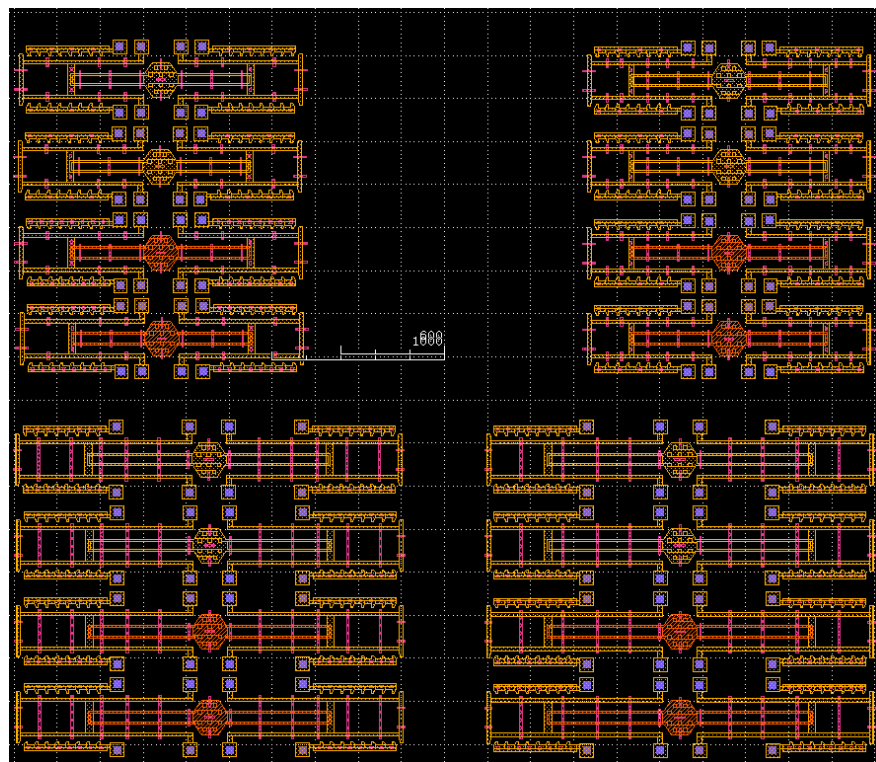


Figure 3.14 - Design Layout 1

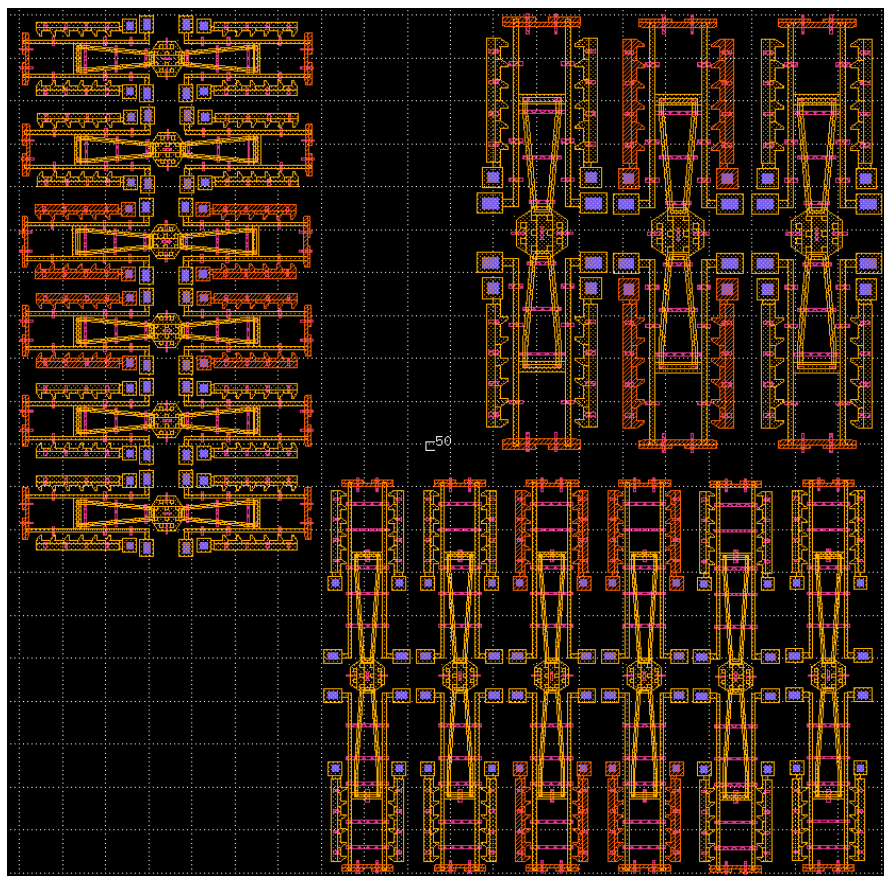


Figure 3.15 - Design Layout 2

4.0 Test Plan

The test plan for our mechanism revolved around four main points of interest:

1. The resistance of the mechanism.
2. The optimal overall length (L) of each cantilever.
3. The optimal placement of the cross-beam.
4. The optimal tip displacement of the cantilever.

Measuring the resistance of our mechanism under no fluid flow will provide a reference point in order to calculate the velocity of a fluid. Knowing that, as the velocity of a fluid increases the resulting temperature of the platform which the fluid is flowing over will decrease due to convection losses. This resulting decrease in temperature will cause a measurable decrease in resistance, similar to how a thermistor works, but more precise to changes due to the microscopic size and thermal scaling properties. The change in resistance can then be used to formulate an equation to measure the velocity of a fluid. A similar device uses hot wire anemometry with expensive and hard to fabricate metal connections. The goal is to raise our thermistor unit above the boundary layer of the fluid into linear flow to get an accurate measurement when the flow changes. In order to raise our thermistor unit above the boundary layer of the fluid we look at three main parameters; overall length of each cantilever, placement of the cross-member, and the overall displacement of the tip of the cantilevers.

Measuring the resistance of the mechanism:

1. Create buckle in cantilever
 - i. Displace the tip of one of the cantilevers into the next locking position.
 - ii. Displace the other tip of the cantilevers into the next locking position.
2. Using a 4 point probe, measure the resistance of the mechanism
 - i. Set the power supply to a constant voltage.
 - ii. Turn off power supply.
 - iii. Place probes on the anchors of the mechanism.
 - iv. Turn on power supply
 - v. Use another set of probes to measure/record the resulting current.
3. Determine if the tip of the cantilever can be displaced any more
 - i. Yes: Go back to 1.
 - ii. No: Stop.

Determining the optimal length of each cantilever:

1. Create buckle in cantilever
 - i. Displace the tip of one of the cantilever into the next locking position.
 - ii. Displace the other tip of the cantilever into the next locking position.
2. Determine height displacement of platform.
3. Determine if the tip of the cantilever can be displaced any more
 - i. Yes: Go back to 1.
 - ii. No: Stop.

Determining the optimal placement of the cross-member:

1. Create buckle in cantilever
 - i. Displace the tip of one of the cantilevers into the next locking position.

- ii. Displace the other tip of the cantilevers into the next locking position.
- 2. Determine height displacement of platform
- 3. Determine if platform displaced in desired direction
- 4. Determine if the tip of the cantilever can be displaced any more
 - i. Yes: Go back to 1.
 - ii. No: Stop.

Determining the optimal tip displacement of the cantilever:

- 1. Create buckle in cantilever
 - i. Displace the tip of one of the cantilevers into the next locking position.
 - ii. Displace the other tip of the cantilevers into the next locking position.
- 2. Determine height displacement of platform.
 - i. If the platform goes out of focus (increases in height): Go back to 1.
 - ii. If the platform stays in focus (no change in height): Stop

5.0 Results

The first round of testing proved to be quite successful, and also revealed opportunities to improve. Mechanically, the design was able to be fully demonstrated. As seen in Figures 6.1 and 6.2, the platform has been raised above the substrate and the locking bars are securely held by the ratcheting arms. Use of nearly all ratchet teeth was feasible to adjust the height of the platform.

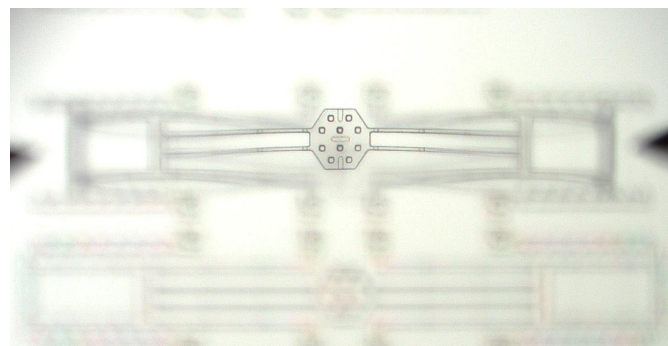


Figure 5.1: Activated Structure (platform focal view)

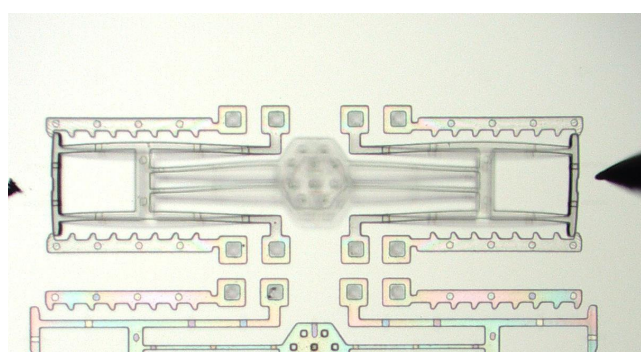


Figure 5.2 - Activated Structure (Base focal view)

The modes of failure of the first round of fabrication were largely due to the flexibility of the locking bar, and lack of interaction between the locking bar and the ratchet teeth. The photo

below shows a partially constructed structure. As the needle is used to push the bar past the teeth on one side, the bar tilts to the side and separates from the opposing tooth. This made the construction of the parts more time consuming.

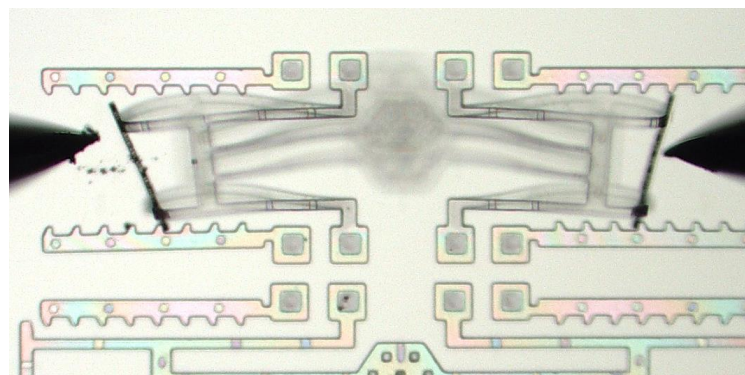


Figure 5.3 - Partially constructed structure (Base focal view)

The second round of fabrication brought more challenges. With the changes made to the design, fractures in the locking bar were frequent (seen below). This change was initially made to increase rigidity, however it also increased the effect of a stress concentration at the center notch.

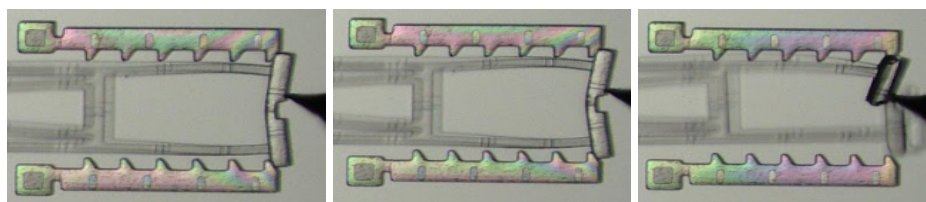


Figure 5.4 - Stress concentration at notch

One structure with the gold coating was successfully erected which allowed us to test the electrical/thermal properties of this design, and attempt to validate parts of our design goal; create a microfluidics boundary layer analysis structure.

Current was applied to the structure via the substrate anchors. Once a steady state current was achieved, forced convection was created over the device while monitoring the current draw. 0.98 Volts at 6 mA was initially applied. The current fluctuated $\pm 1\text{mA}$ during these tests, which is promising but is not a conclusive result. Another consideration is that heat is generated in the area of minimal resistance. In the case of our structure that is in the beams that lift the platform, rather than the platform itself. Some tweaks could be made to the structure to increase its functionality at heat dissipation. A common sensor used is a thin wire anemometer, which has a similar operational theory as our device, lifting an object to be cooled by air above the boundary layer, but in this case it uses a thin metal wire rather than a platform, and uses a heated cantilever on either side to lift the wire:



Hot-Wire Anemometry



- MEMS technology is ideally suited to overcome both of these limitations.

44

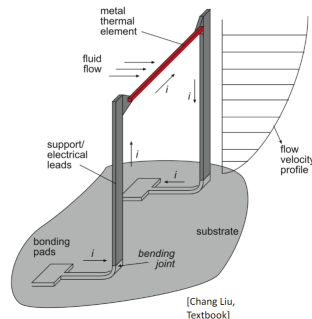


Figure 5.5 - Hot-Wire Anemometry

The resistance of a thermal element is defined as: $R = Ro (1 + \alpha(T - To))$, and the thermal loss can be modeled based on airflow via forced thermal convection. This equation can be difficult to analyze since it involves unstable variables. Consequently, our plan was to develop a baseline by measuring resistance at known airflow velocities, and use machine learning to then predict the airflow based on resistance using interpolation.

Our project focused on having a stable platform with adjustable height which is easy to produce and assemble. This means a thin metal wire cannot be used. However, the beams leading to the platform can be made significantly narrower than the rest of the structure and have a similar effect as this will result in more of the heat being dissipated in the parts of the structure above the boundary layer. Keeping the overall resistance of the structure the same, the internal part with the highest resistance will need to dissipate the most heat as $P = I^2 * R$.

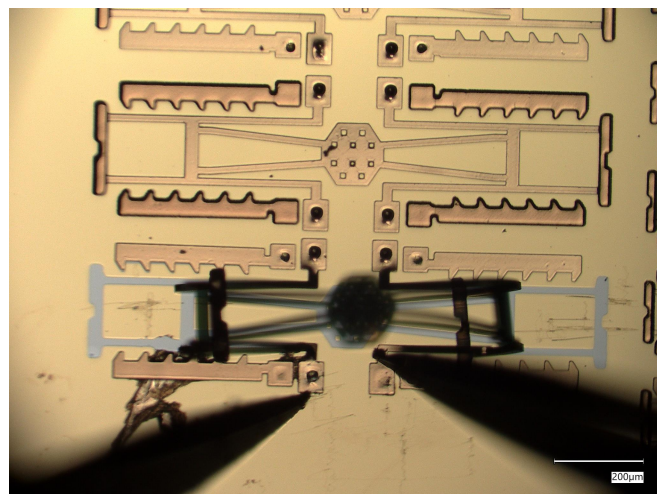


Figure 5.6 - Measurement of Resistance for Activated Gold Plated Structure

This can be modeled as three resistors in series, one increasing in resistance to model how the heating effect due to amperage will increase the resistance, one decreasing

proportionally to represent the cooling due to airflow, and one to model the parts of the structure under the boundary layer that are not meaningfully affected. The green lines on the graph represent energy levels increasing due to more power being supplied, and blue represent increased cooling due to higher airspeeds. As we see we get meaningful, somewhat linear value lines representing power being dissipated across the larger resistor, which is the thin arms supporting our platform without the cooling effect that increases directly proportional to the heating increasing. We can then measure the change in amperage, at each stage with known airflow and then linearly interpolate to create a prediction of airspeed. By decreasing the resistance of the arms we are increasing the sensitivity of our structure. We can choose one of the straight green lines to measure, and see how much the blue tries to change it. The energy line followed would depend on the expected airflow, as too much power will burn the resistor, and too little will overcool it. Figure 5.8 shows the model without the airflow to cool the resistor, which would result in the resistor burning up before it had a meaningful change.

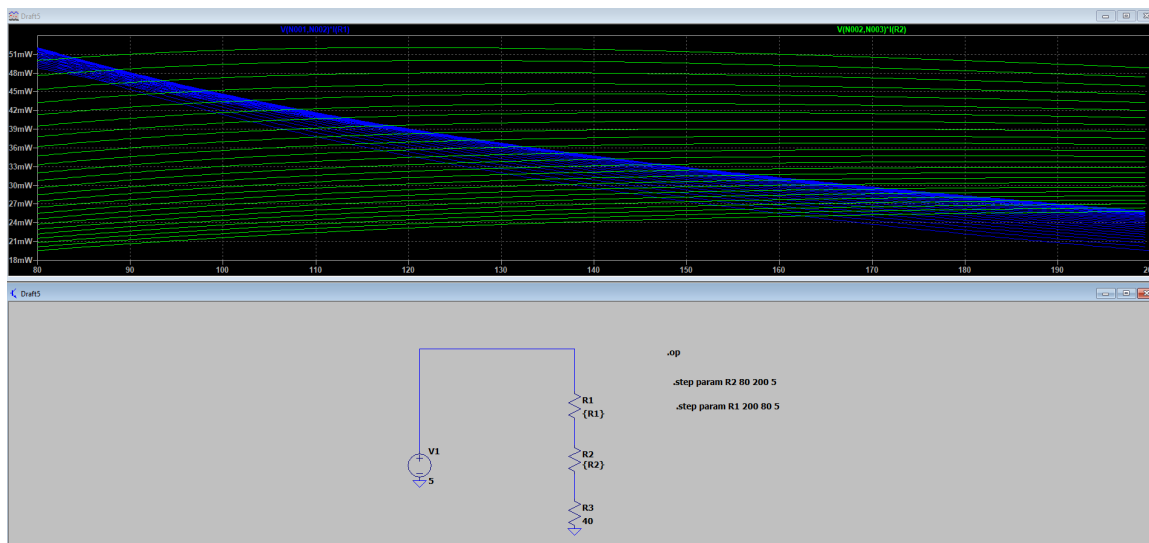


Figure 5.7 - Power Dissipation Model

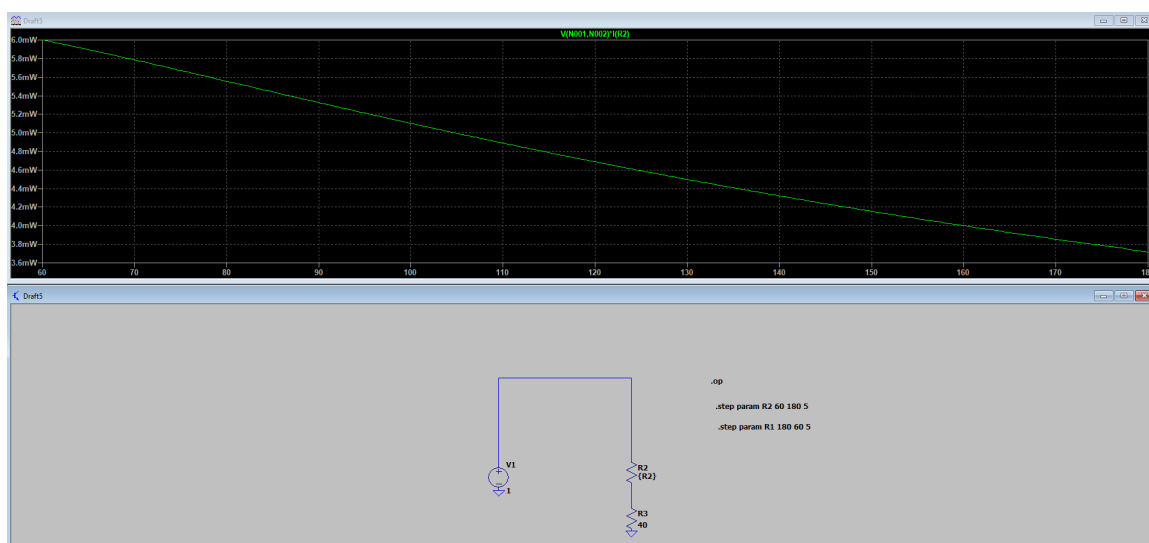


Figure 5.8 - Power Dissipation Model Without Cooling

6.0 Conclusion and Lessons Learned

To sum up the information presented above, our exploration into MEMS aimed at developing a deployable system for gauging fluid velocity across a surface that has yielded valuable insights and both successes and challenges.

The initial testing phase demonstrated mechanical functionality, successfully elevating the platform above the substrate using the interlocking cantilevers and ratcheting arms. Notably, the design allowed for the utilization of nearly all ratchet teeth for precise height adjustments. However, the first round of fabrication exposed limitations, primarily stemming from the flexibility of the locking bar and insufficient interaction with the ratchet teeth. Construction complexities arose as the bar tilted and separated during the engagement process, prompting a need for refinement.

The second round of fabrication, while introducing improvements, brought new challenges. Modifications aimed at increasing rigidity inadvertently led to frequent fractures in the locking bar, indicating high stress concentrations at the center notch. This underlines the delicate balance required in adjusting design parameters and the need for meticulous consideration of material properties.

It should be noted that in our first design the placement of the crossbeam was varied in order to determine if it would help reduce the maximum stress experienced at locations with a high stress concentration. Ultimately it was found that the stress was not an issue during this stage of the design. Moving forward it was decided to proceed with the placement that maximized height. Had these cross beam placement iterations been implemented in our second mask, there may have been fewer breakages at that spot. This outlines how sometimes it is important to reflect on previous design changes before deciding to proceed with the newest iteration.

Despite challenges, a structure with a gold coating was successfully assembled, enabling the testing of electrical and thermal. Initial results from current application and forced convection were promising, showing a fluctuation of $\pm 1\text{mA}$. However, further analysis is necessary for conclusive outcomes.

Lessons Learned:

- Striking the Right Balance: Navigating the delicate equilibrium between flexibility and rigidity, especially in pivotal components (like the locking bar), emerges as a critical consideration in optimizing MEMS functionality.
- Understanding Interactions: Recognizing the intricate interplay between design elements is imperative. Every alteration made to one facet of the design should be comprehensively assessed for its holistic impact on the structure's performance.
- Mitigate Material Stress: Unforeseen stress concentrations, a consequence of well-intentioned enhancements, underscore the need for a thorough analysis. It's a reminder that even the most thoughtful design adjustments can introduce subtle challenges that demand careful consideration.

- Refinement through Iteration: Embracing the iterative nature of design and fabrication demands a systematic and strategic approach. Insights gathered from each iteration serve as the foundation for enhancement and innovation.
- Fabrication: If you have a design that works as intended, include it in future iterations. This practice ensures that any failures in the new design can be attributed to specific changes rather than potential fabrication shortcomings.

In closing, our project not only advanced our understanding of MEMS but also emphasized the importance of meticulous design considerations and iterative refinement. These lessons will undoubtedly contribute to the future success of similar endeavors and pave the way for more effective MEMS technologies.

7.0 References:

Johnstone, R. W., Ma, A. H., Sameoto, D., Parameswaran, M., & Leung, A. M. (2008). *Buckled cantilevers for out-of-plane platforms*. Journal of Micromechanics and Microengineering. <https://doi.org/10.1088/0960-1317/18/4/045024>

Sturm, H., Dumstorff, G., Busche, P., Westermann, D., & Lang, W. (2012). Boundary layer separation and reattachment detection on airfoils by thermal flow sensors. *Sensors*, 12(11), 14292–14306. <https://doi.org/10.3390/s121114292>

8.0 Appendix:

Stiffness Increase by Changing Thickness:

$$\begin{aligned} (t_{new})^3 - (t_{old})^3 / (t_{old})^3 * 100 &= \text{percent increase} \\ (50E^{-6})^3 - (20E^{-6})^3 / (20E^{-6})^3 * 100 &= 1462.5\% \end{aligned} \quad (\text{Equation 8.1})$$